# NUMERICAL SIMULATION OF A PARABOLIC TROUGH SOLAR COLLECTOR CONSIDERING THE CONCENTRATED ENERGY FLUX DISTRIBUTION

**Ahmed Amine Hachicha, Ivette Rodríguez, Roser Capdevila and Assensi Oliva**

Centre Tecnològic de Transferència de Calor (CTTC)
Universitat Politècnica de Catalunya (UPC)
ETSEIAT, C. Colom 11, 08222 Terrassa (Barcelona), Spain
Fax: +34 93 739 89 20 e-mail: cttc@cttc.upc.edu

## 1. Introduction

Concentrated solar power plants are one of the most promising renewable options for electric generation. Nowadays, parabolic trough collectors (PTC) are the most proven, widespread and commercially tested technology available for solar harnessing (Price et al. 2002).

Most of the parabolic trough plants deployed operate between 290 and 390ºC using oil as heat transfer fluid (HTF). A PTC is constructed as a long parabolic mirror with a dewar tube running its length in the focal line. The HTF runs through the tube and absorbs the concentrated sunlight. The surface of the receiver is covered with a selective coating which has a high absorptance for solar radiation but low emittance for thermal radiation. A glass envelope is used around the receiver tube to reduce the convective heat losses with vacuum or air in the space between the receiver and the cover. The PTC is aligned to the north-south axis and tracks the Sun from east to west as it moves across the sky using a tracking mechanism system.

Many works have been carried out to study and model PTCs. Sandia National laboratories performed tests to determine the thermal losses and thermal efficiency of the PTC used in LS2 Solar Thermal Electric Generation Systems (SEGS). Dudley et al. (1994) proposed a one-dimensional (1D) model to analyse the thermal behaviour and performance of the LS2 SEGS collector under different receiver configurations and two selective coatings by comparing with experimental data. Froristall (2003) developed and analysed both a 1D and a two-dimensional (2D) heat transfer model of the PTC. A direct steam generation (DSG) collector model was proposed by Odeh et al. (1998) based on the absorber wall temperature rather than the working fluid temperature. García-Valladares and Velázquez (2009) proposed a numerical simulation of the optical, thermal and fluid dynamic behaviour of a single-pass solar PTC and then extended the study to counter flow concentric circular heat exchangers.

The majority of the published studies about the heat transfer process in the PTC have established to calculate the heat losses and thermal performance by considering the solar radiation as a constant and neglecting the heat flux distribution around the receiver surface. Some optical models for determining the optical behaviour of a PTC rely on analytical techniques (Jeter 1987) while most use ray-tracing techniques to evaluate the optical efficiency. Guven and Bannerot (1985) have presented an optical model which uses a ray-tracing technique to evaluate the optical performance. Y-L He et al. (2011) used the Monte Carlo Ray-tracing Method (MCRT). The Monte Carlo Method is a statistical method that requires knowledge that is quite different to Computational Fluid Dynamics (CFD) and is complicated in formulation and resolution even for simple problems (Modest 1993). On the other hand, the finite volume method (FVM) proposed by Raithby and Chui (1990) is one of the most popular methods used in CFD. It has been extensively applied at different situations because it leads to the exact satisfaction of the conservation laws.

The aim of this study is to develop a heat transfer model for a PTC in order to characterize its performance by considering the energy flux distribution around the collector. This is done by means of an energy balance model based on finite volume techniques. An unstructured formulation has been used with the FVM to solve the Radiative Transfer Equation (RTE) between the parabola and the heat collector element (HCE) to determine the concentrated solar energy flux. The numerical model has been validated with numerical and experimental results.

## 2. PTC mathematical model

The general modelling approach is based on an energy balance about the HCE. It includes the direct normal solar irradiation, the optical losses from both the parabola and the HCE, the thermal losses from the HCE,

and the gains into the HTF.

Different assumptions and constraints are adopted:

- One dimensional, single phase (liquid) and steady state incompressible flow is considered.
- Fluid velocity is assumed constant through the absorber tube.
- The fluid thermal-physical properties are function of temperature.
- Optical properties are independent of temperature except for the selective coating emissivity.
- Heat conduction along the support bracket is neglected.
- Heat conduction in the absorber tube and glass cover is considered in the axial and azimuthal directions.
- Thickness of the absorber and glass cover are negligible.
- Wind direction is normal to the axis of the HCE.
- No participating medium with diffuse reflections and irradiation is considered between the absorber tube and glass cover.
- Thermal radiation between the HCE and the parabolic trough is neglected.
- The glass envelope is considered opaque to infrared radiation.
- Optical errors due to imperfections that may result from poor manufacturing and/or assembling, imperfection tracking of the sun, and/or poor operating conditions are neglected.
- The effective solar irradiation is considered as totally absorbed by the absorber selective coating since the absorption in the envelope is neglected (solar absorptance about 0.02).

### *2.1 Solar irradiation analysis*

The solar irradiation is modelled as a collimated beam without taking into account the influence of the finite size of the Sun (Riveros and Oliva 1986). The collimated beam is solved through its path to the absorber tube. The direct part of the solar irradiation is only considered as it is several times higher than the diffuse one.

The RTE for a gray absorbing, emitting and scattering medium at the position r and the direction $\hat{s}$ may be written as

$$\frac{dI(r,\hat{s})}{ds} = \kappa(r) I_b(r,\hat{s}) - \beta(r) I(r,\hat{s}) + \frac{\sigma_s(r)}{4\pi} \int_{4\pi} I(r,\hat{s}') \Phi(\hat{s}',\hat{s}) d\Omega' \quad \text{(eq.1)}$$

where $I(r,\hat{s})$ is the radiative intensity at the position $(r,\hat{s})$, $\kappa(r)$ and $\sigma_s$ are the absorption and scattering coefficients, respectively. $\Phi(\hat{s}',\hat{s})$ is the scattering phase function and $I_b$ is the Planck black body intensity. The two coefficients are related by means of the extention coefficient $\beta = \kappa + \sigma_s$. In the present work, the medium is assumed transparent and no participating so that $\kappa = 0$ and $\sigma_s = 0$ leading to the simple equation 2.

$$\frac{dI(r,\hat{s})}{ds} = 0 \quad \text{(eq.2)}$$

The mirror is assumed to be totally specular reflecting for solar irradiation and opaque surface. The boundary condition of eq.1 for a diffuse emission, specular reflecting opaque surface is given by (Modest 1993)

$$I(r_w,\hat{s}) = \varepsilon(r_w) I_b(r_w) + \frac{\rho^d(r_w)}{\pi} \int_{\hat{n}\cdot\hat{s}'<0} I(r_w,\hat{s}') \left|\hat{n}\cdot\hat{s}'\right| d\Omega' + \rho^s(r_w) I(r_w,\hat{s}_s) \quad \text{(eq.3)}$$

where $\hat{s}_s$ is the specular direction defined as the direction from which the light beam must hit the boundary in order to travel into the direction of $\hat{s}$ after a specular reflection. This direction is determined by the reflection law

$$\hat{s}_s = \hat{s} - 2(\hat{s}\cdot\hat{n})\hat{n} \quad \text{(eq.4)}$$

$\rho^d$ is the diffuse fraction of reflected energy and $\rho^s$ is the specular reflection fraction, thus $\rho = \rho^d + \rho^s$. In this case $\rho = \rho^s$ for the mirror. Optical properties are obtained from the literature (Dudley et al. 1994)

according to the specifications defined by the manufacturer and determined at zero incident angle.

The solar energy flux absorbed $q_{SolAbs}$ is obtained by angular integration of the solar flux around the absorber tube.

$$q_{SolAbs} = \int_{4\pi} I(\hat{s} \cdot \hat{n}_i) d\Omega \quad \text{(eq.5)}$$

The solar irradiation analysis should provide the heat flux distribution around the HCE, but also the optical efficiency of the PTC. It is defined by the ratio of solar energy falling on the surface of the absorber tube to that which falls on the reflective surface of the collector.

$$\eta_{opt} = \frac{q_{3SolAbs}}{q_{inc}} \quad \text{(eq.6)}$$

The solar heat flux distribution is usually expressed by a parameter called Local Concentration Ratio (LCR) (Jeter 1987) which presents the ratio of the concentrated solar flux at the absorber surface to the incident solar radiation.

$$LCR = \frac{q}{q_{inc}} \quad \text{(eq.7)}$$

The LCR depends on the azimuthal angle $\phi$, the incident angle and the collector geometric parameters involved in the solar concentration. The relative size of the absorber is described by the geometrical concentration ratio, which is defined as the ratio between the projected aperture area to the absorber area (Rabl, 1987). Integrating the flux distribution over the entire absorber and dividing by the incidence irradiance yields the interceptance

$$\gamma = \frac{\int q\, r\, d\phi}{q_{inc} w} = \frac{\int LCR\, r\, d\phi}{w} \quad \text{(eq.8)}$$

where $r$ is the receiver radius and $w$ is the collector aperture. This ratio is defined as the fraction of the reflected radiation that is incident on the absorbing surface of the receiver. It is of interest in concentrating systems design as it contains the effect of all optical errors.

### *2.2 Energy balances in the HCE*

The energy balance model of the HCE includes the heat transfer from the HTF to the ambient through both, the absorber tube and the glass envelope. For this purpose, the HCE is divided into $n_x$ longitudinal and $n_\phi$ circumferential control volumes. The HTF is only discretised in the longitudinal direction. Both, temperatures and heat fluxes, vary along the circumference and the length of the HCE except for the fluid which varies only along the length of the absorber. By applying the energy conservation principle to the control volumes of the HCE, the energy balance equations are determined.

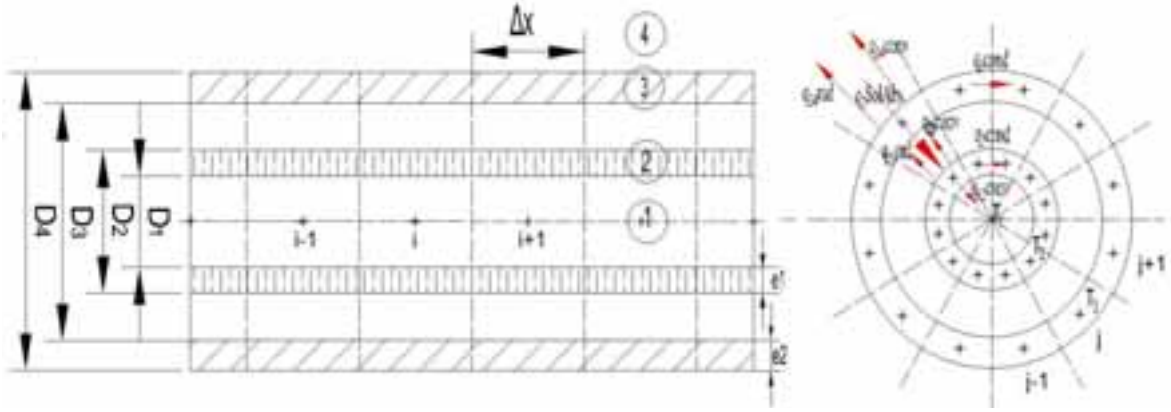


**Fig.1: Spatial discretisation of the HCE: left longitudinal section, right azimuthal section (1-HTF, 2- absorber surface, 3- glass cover, 4- environment)**

The energy balance model provides the temperature distribution of the HTF, the receiver tube and the glass cover. The model also determines the performance of a PTC by calculating the useful energy, the thermal losses and the thermal efficiency. The PTC thermal efficiency can be obtained by dividing the useful energy per receiver length $q_u$ by the direct normal solar irradiation $I_b$ at the collector aperture per receiver length. The PTC thermal efficiency is determined as

$$\eta_{th} = \frac{q_u}{A_a I_b} \quad \text{(eq.9)}$$

being $A_a$ is the aperture area.

Applying the energy equation to the HTF with the aforementioned hypotheses and assuming that enthalpy gradient can be evaluated as a function of the average specific heat and the temperature difference between the inlet and outlet of the control volume, the energy balance at each control volume reads, (see fig.1 for nomenclature)

$$\sum q_{12conv,j}\Delta x \simeq \dot{m}\left[h_{out,i} - h_{in,i}\right] \simeq \dot{m}\,\overline{C_{p,i}}\left[T_{out,i} - T_{in,i}\right] \quad \text{(eq.10)}$$

The useful energy is obtained by summing the heat gained by the HTF along the absorber. Thus,

$$q_u = \sum_i \sum_j q_{12conv,j} \quad \text{(eq.11)}$$

The energy equation is also applied to the glass cover and to the absorber control volumes. In the next sections, the heat fluxes equations are shown. The heat losses are the sum of the convective and radiative flux lost to the surroundings.

$$q_{heatloss} = \sum_i \sum_j (q_{34conv,j} + q_{34rad,j}) \quad \text{(eq.12)}$$

### *2.2.1 Convection heat transfer between the HTF and the absorber*

The convection heat transfer between the HTF and the absorber metal pipe is evaluated according to the Newton's law of cooling. For a jth term :

$$q_{12conv,j} = \frac{h_1 \pi D_1}{n_2}(T_{2,j} - T_1)\Delta x \quad \text{(eq.13)}$$

where $h_1$ is the HTF convection heat transfer coefficient at $T_1$ which is evaluated as a function of the Nusselt number $Nu_{D_1}$. As a first approximation, correlations for isothermal cylinders (Incropera and DeWitt, 1990) are used to evaluate the Nusselt number taking into account the temperature of the cylinder sectors. The Nusselt number is calculated using the Dittus-Boelter equation, $Nu_{D_1} = 0.023 Re_{D_1}^{4/5} Pr^m$, (where $m$=0.4 for heating the HTF and $m$=0.3 for cooling the HTF). With high temperature difference between the HTF bulk temperature and the absorber temperature (more than 10 ºC), the Sieder-Tate correlation is used as it can be more accurate and it takes into account the change in viscosity due to temperature change. This expression reads, $Nu_{D_1} = 0.027 Re_{D_1}^{4/5} Pr^{\frac{1}{3}} \left(\frac{\mu}{\mu_s}\right)^{0.14}$ (where $\mu$ and $\mu_s$ are the fluid viscosities evaluated at the bulk and at the heat-transfer boundary surface temperatures, respectively).

### *2.2.2 Conduction heat transfer through the absorber wall and the glass envelope*

The energy rate per unit length conducted across the cylindrical wall of a solid is defined by

$$q_{cond,j} = -k\frac{dT}{r d\theta} e_{1/2}\Delta x \quad \text{(eq.14)}$$

For the azimuthal direction and for for the longitudinal direction as

$$q_{cond,i} = -k\frac{dT}{dx} A_x \quad \text{(eq.15)}$$

where $A_x$ is the frontal area of the nodal section.

### 2.2.3 Convection heat transfer between the absorber and the glass envelope

The annular region can be assumed as a good vacuum and then the convection heat transfer in the energy balance is ignored. However, in operational solar plants the vacuum condition in the annulus can be changed or damaged by broken seals, hydrogen penetration and getter decomposition when vacuum fails. In those cases, $q_{23conv}$, which can be free molecular convection or natural convection (Ratzel et al 1979), should be considered.

$$q_{23conv,j} = \frac{\pi D_2}{n} h_{23}(T_{2,j} - T_{3,j})\Delta x \quad \text{(eq.16)}$$

If free molecular convection is considered, the heat transfer coefficient is evaluated as,

$$h_{23} = \frac{k_{std}}{(D_2/2ln(D_3/D_2) + b\lambda(D_2/D_3 + 1))} \quad \text{(eq.17)}$$

$$b = \frac{(2-a)(9\gamma - 5)}{2a(\gamma + 1)} \quad \text{(eq.18)}$$

$$\lambda = \frac{2.33 * 10^{-20}(T_{23} + 273.15)}{P_a \delta^2} \quad \text{(eq.19)}$$

where $k_{std}$ is the thermal conductivity of the annulus gas at standard temperature and pressure, $b$ the interaction coefficient, $\lambda$ the mean-free path between collisions of a molecule, $a$ the accommodation coefficient, $\gamma$ the ratio of specific heat for the annulus gas, $T_{23}$ the average temperature of the gas in the annulus $(T_{2,j} + T_{3,j})/2$, $P_a$ the annulus gas pressure and $\delta$ molecular diameter of the gas (air and hydrogen have molecular diameters of $3.53 \times 10^{-8}$ and $2.32 \times 10^{-8}$ respectively).
In the case of consider the natural convection within the annulus, then the heat transfer coefficient is evaluated as,

$$h_{23} = \frac{2k_{eff}}{D_2 ln(D_3/D_2)} \quad \text{(eq.20)}$$

being the effective thermal conductivity of the gas $\left(k_{eff} = k(0.386)\left[\frac{Pr}{0.861 + Pr}\right]^{0.25}(Ra_c)^{0.25}\right)$ function of its thermal conductivity $k$, and the Rayleigh number $\left(Ra_c = \frac{(ln(D_3/D_2)^4}{L^3[D_2^{-0.6} + D_3^{-0.6}]^5} Ra_L\right)$. $Ra_L$ is evaluated at the air gap distance of $(D_3 - D_2)/2$.

### 2.2.4 Radiation heat transfer between the absorber and the glass envelope

The surfaces have been considered as gray and diffuse emitters, absorbers and reflectors. The glass envelope is assumed to be opaque to the infrared radiation. For simplicity and according to the spatial discretisation, the radiation in the jth control volume can be approximated as

$$q_{23rad,j} = \frac{1}{n}\left(\frac{\sigma\pi D_2(T_{2,j}^4 - T_{3,j}^4)}{\frac{1}{\varepsilon_2} + \frac{D_2(1-\varepsilon_3)}{D_3\varepsilon_3}}\right)\Delta x \quad \text{(eq.21)}$$

where $\varepsilon_2$ is the emittance of the absorber tube and $\varepsilon_3$ is the emittance of the glass envelope.

### 2.2.5 Convection heat transfer from the glass envelope to the atmosphere

The convection heat transfer from the glass envelope to the ambient is evaluated according to,

$$q_{34conv,j} = h_{34} \frac{\pi D_4}{n} (T_{3,j} - T_{amb}) \Delta x \quad \text{(eq.22)}$$

The heat transfer coefficient, $h_{34}$ , is evaluated from the Nusselt number depending whether the convection is natural or forced as: $Nu_{D_4} = 0.48 Ra_{D_4}^{0.25}$ or $Nu_{D_4} = 0.193 Re_{D_4}^{0.618} Pr_5^{1/3}$ , respectively.

### *2.2.6 Radiation heat transfer between the glass envelope and the sky*

The glass envelope is assumed to be a small convex grey object in a large black body cavity (the sky). By applying the net radiation method, the radiation between the glass envelope and the sky is written as

$$q_{34rad,j} = \varepsilon_4 (T_{3,j}^4 - T_{sky}^4) \frac{\pi D_4}{n_p} \Delta x \quad \text{(eq.23)}$$

### *2.2.7 Solar irradiation absorption*

The distribution of the solar irradiation absorbed by the receiver tube $q_{2Solabs,j}$ is calculated by means of the methodology as described in (2.1). The total solar absorbed flux $q_{SolAbs}$ is calculated as

$$q_{SolAbs} = \sum_j q_{solar,j} \quad \text{(eq.24)}$$

## 3. Numerical Solution

The energy balance equations result in a set of non-linear algebraic equations which are solved using an iterative procedure where temperatures and heat fluxes are coupled. The equations of the HCE (see eq.11) are discretised in a linear system and then solved with a direct solver (LU decomposition). The temperature at the faces of the control volumes are evaluated by means of a high order scheme (SMART). The concentrated solar distribution is conducted by a FVM code for solving three-dimensional (3D) unstructured mesh. A 3D structured, non orthogonal and non-overlapping grid is used to descritise the domain between the parabola and the receiver tube which is a particular case of the 3D unstructured mesh. The domain is reduced to the half because of the symmetry around the z axis. The angular space (4π) is subdivided into $N_\theta \times N_\varphi = M$ non-overlapping control angles, where $\theta$ is a polar angle ranging from 0 to π and $\varphi$ an azimuthal angle ranging from 0 to 2π (see figure 2).

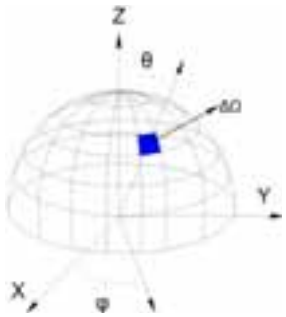


**Fig.2: Angular discretisation**

In order to reduce the false scattering, one of the shortcomings of the FVM, which is due to the spatial discretisation errors, the mesh is arranged to follow the direction of the reflected rays. The number of directions in the azimuthal direction is chosen according to the spatial discretisation along the parabola and adjusted to capture the direction of the specular reflection. The angular mesh contains all the directions of the reflection focused on the focal point of the parabola.

The angular discretisation is arranged to capture the collimated incidence which comes from the sun irradiation (Chai et al. 1994). The collimated intensity is solved directly by the FVM. The angular space between two consecutive reflection directions is filled with an extra direction. Thus, the RTE for a transparent medium is integrated over the control volume $\Delta V$ and over each of the solid angle elements $\Delta\Omega$. The STEP scheme is used to relate the control volume facial intensity to the nodal one. This

scheme is analogous to the upwind scheme used in a CFD code.

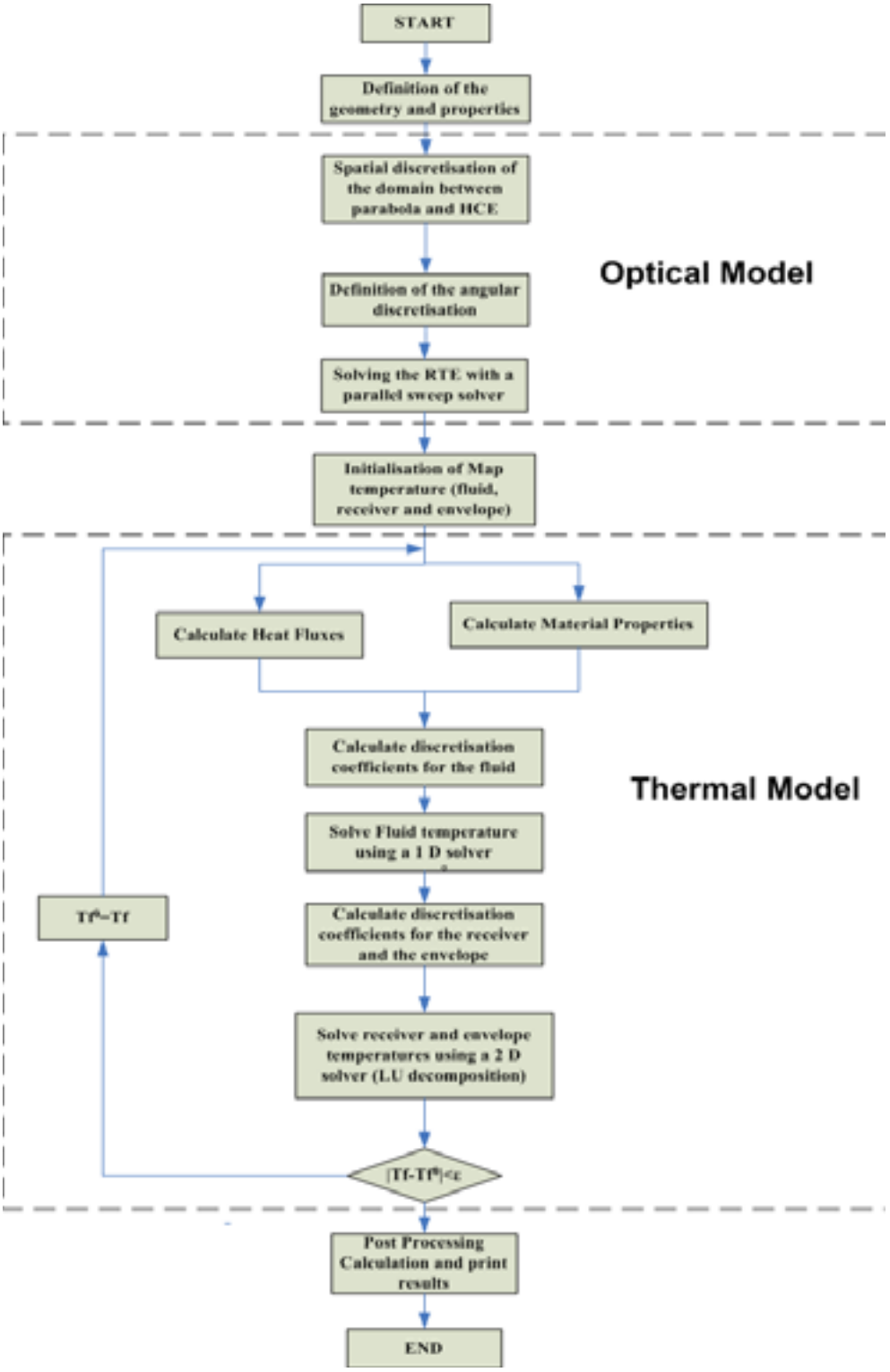


**Fig.3: Flowchart of the general algorithm**

The discretised algebraic radiative transfer equations and boundary conditions are solved by means of a parallel sweep solver (Colomer et al, 2010). The calculation of the solar concentrated distribution is carried out as a pre-processing task using the optical properties of each surface. The above described methodology gives as a result the distribution about the absorber tube of the radiative heat flux. This heat flux distribution is added to the energy balance model as a boundary condition of the outer surface of the absorber tube. The

resulting heat flux distribution from the resolution of the RTE is integrated over the boundary of each control volume of the absorber tube.

In the energy balance model, there is another coupling between the one dimensional model for the HTF in the longitudinal direction of the PTC and the two dimensional model for the HCE. The energy equation has been solved in the HTF by integrating the total convective heat flux transferred from the absorber tube to the HTF. The temperature of the HTF is then determined using a direct solver (TDMA) method in the longitudinal tube direction.
The general algorithm, as can be seen in figure 3 is divided in two steps: the optical model or the pre-processing calculation of the concentrated solar flux distribution and the thermal model for modelling the HCE.

## 4. Computational results and validation

In order to validate the optical model, simulations results are compared first with semi-analytical results of Jeter (1987) and then with numerical results of Cheng et al. (2010) which are obtained with the MCRT method. The geometric shape of the PTC (Model 3001-03) used by Jeter (1987) is reproduced. Jeter considered the influence of the finite size of the sun, “the cone optics”, which is not considered in our numerical results. This phenomenon causes a spreading of the reflected incident radiation around the absorber (Riveros and Oliva 1986) and can not be considered by assuming the solar radiation as a collimated beam.

Figure 4 presents the comparison of the LCR obtained by the optical model and the analytical results of Jeter (1987). It can be seen that increasing the number of nodes in the azimuthal direction of the absorber, the false scattering decreases. The main difference between the present results and the results of Jeter is the influence of the finite size of the sun which tends to moderate the solar flux distribution around the absorber and the false scattering. This is why the maximum obtained by the present model seems to be higher when decreasing the false scattering.

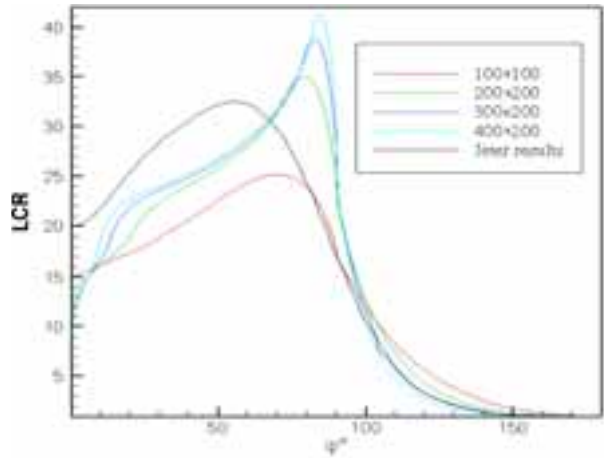


**Fig.4: LCR distribution for different meshes and comparison with Jeter**

The optical model has been also verified with the numerical results of Cheng et al. (2010) for a typical LS-2 PTC module which has been tested by Dudley et al.(1994).
Different grids systems are studied and compared with the MCRT solution (fig.5). The spatial grid system ($n_A$=100, $n_P$=600) has been chosen as the most adequate one because it presents low false scattering and good trend to the results of Cheng where $n_A$ is total number control volumes in the aperture of the parabola and $n_P$ is the total number of control volume in the parabola. The main difference between the present results and those of Cheng is due essentially to the cone optic effect which is taken into account in his paper.

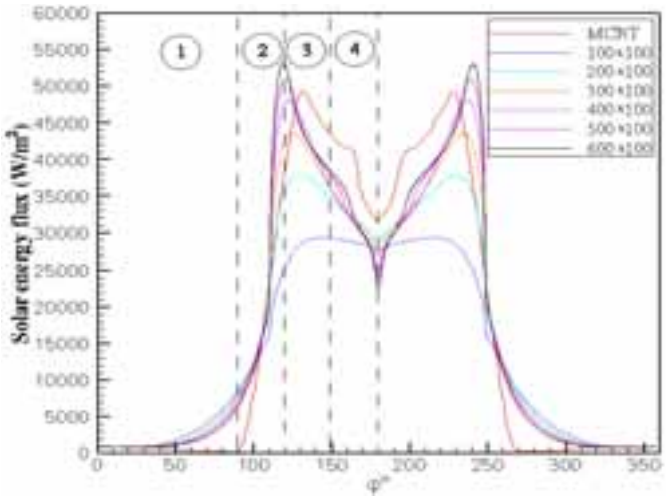


**Fig.5: Solar energy flux distribution around absorber for different grids systems**

As it is shown in fig.5 the solar flux distribution is symmetrical but non-uniform. The curve of solar flux can be divided into 4 zones : i) the direct radiation zone where the absorber tube only receives the direct solar irradiation without concentration, ii) the heat flux increasing zone where the heat flux increase rapidly because of the reflection of the solar irradiation, iii) the heat flux decreasing zone where the reflected solar flux decrease because of the parabolic shape, iv) the shadow effect zone where the heat flux is much lower and decrease rapidly because of the solar irradiation is shadowed by the absorber tube.

Different numbers of longitudinal $n_x$ and azimuthal control volumes $n_\phi$ sections have been tested to get a grid-independent solution. The grid ( $n_x$ =60, $n_\phi$ =60) is considered as grid-independent since there is no significant difference with the finest one.

**Tab. 1: Experimental condition data from Dudley et al. (1994).**

| Test Condition | $I_b$ ($Wm^{-2}$) | $\dot{m}$ ($kgs^{-1}$) | $T_{air}$ (°C) | $T_{in}$ (°C) |
|---|---|---|---|---|
| Case 1 | 933.7 | 0.68 | 21.2 | 102.2 |
| Case 2 | 968.2 | 0.65 | 22.4 | 151.0 |
| Case 3 | 982.3 | 0.63 | 24.3 | 197.5 |
| Case 4 | 909.5 | 0.66 | 26.2 | 250.7 |
| Case 5 | 937.9 | 0.62 | 28.8 | 297.8 |
| Case 6 | 813.1 | 0.72 | 25.8 | 101.2 |
| Case 7 | 858.4 | 0.71 | 27.6 | 154.3 |
| Case 8 | 878.7 | 0.70 | 28.6 | 202.4 |
| Case 9 | 896.4 | 0.79 | 30.0 | 250.7 |
| Case 10 | 906.7 | 0.70 | 31.7 | 299.5 |

Figure 6 shows the distribution of the temperature of the whole absorber tube and glass envelope based on the test condition of case 1 (see Table 1 for details). The temperature of the absorber increases with the increase of the axial direction as shown in figure 7 (a) for different azimuthal angles ( $\phi = 0^\circ, 90^\circ$ and $180^\circ$ ).

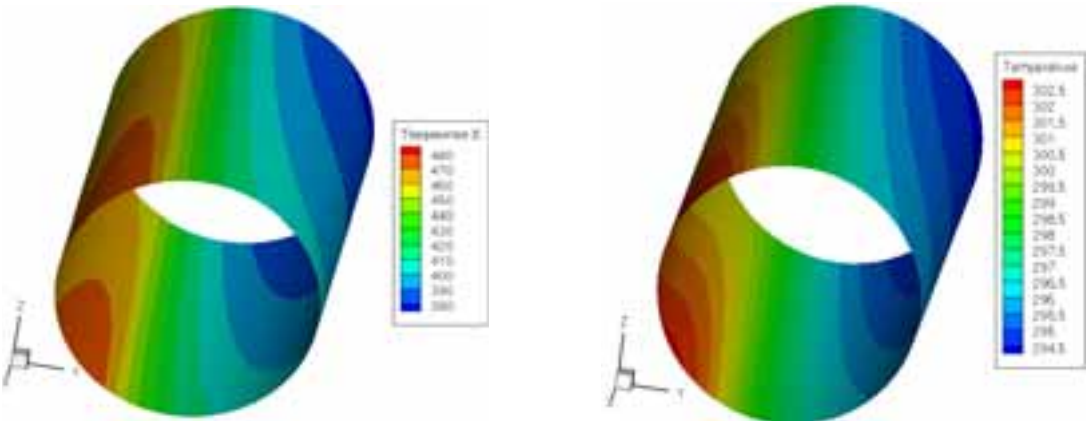

(a) (b)

**Fig.6: Distribution of the temperature of the whole (a) absorber and (b) glass envelope**

It can be seen that the temperature of the absorber at $\phi = 180^{\circ}$ is higher than that of two other angles because the absorber receives more concentrated solar radiation at this angular direction, while at $\phi = 0^{\circ}$ is the lowest one because there is no solar concentration in this direction. The maximum of solar concentration is at about $\phi = 135^{\circ}$. The comparison between the distribution of the temperature of the absorber along the circumferential direction is shown in figure 7 (b) for different axial locations. It can also be seen that the temperature increases with longitudinal direction and the symmetrical distribution of the temperature around the absorber. The distribution of the temperature of the absorber in figure 7 (b) follows the same trend as the solar energy flux distribution. The temperature decrease at $\phi = 180^{\circ}$ which is due to the shadow effect as well as to the optic cone effect.

Several cases (see table 1) have been simulated and compared with experimental results for the cermet (selective coating) with air and vacuum in the annulus space. According to figure 8 (a), the heat losses increase with the fluid temperature which causes the drop of efficiency.

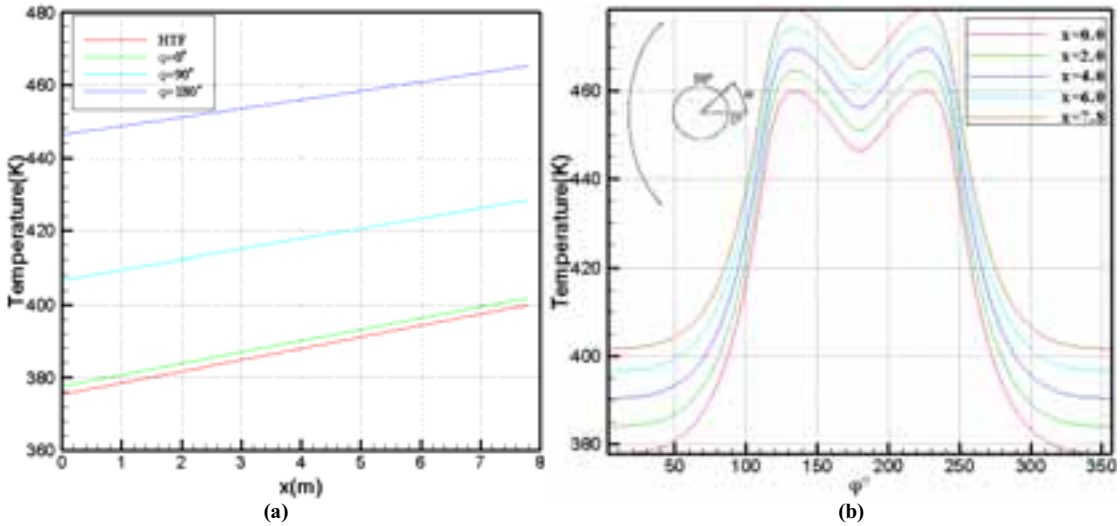


**(a)** **(b)**

**Fig.7 : Variation of the temperature of the absorber (a) with the HTF along the axial direction and (b) azimuthal direction**

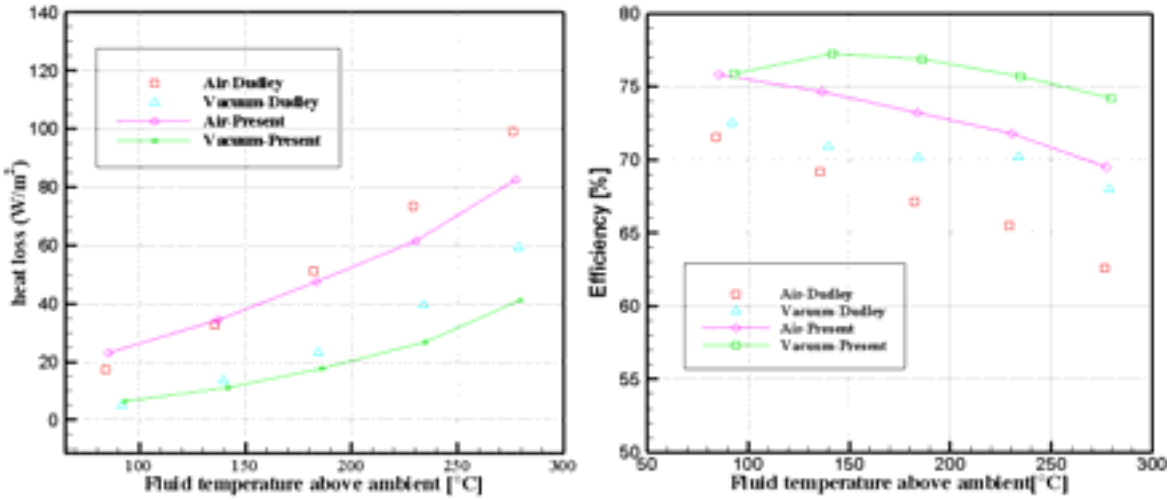


(a) (b)

**Fig.8: Comparison of the (a) heat loss and (b) Efficiency, with experimental results of SNL for air and vacuum in annulus**

The three components of thermal losses (conduction, convection and radiation) vary in different ways depending on the configuration of the receiver. When there is vacuum in the annulus, conduction and convection across the annulus is effectively eliminated. On the contrary. when there is no vacuum, the heat losses increase significantly due to convection and conduction, as expected.

The results follow the same trend as the experimental ones and show a fair agreement in the heat losses especially for low temperatures. However, there is an overestimation of the efficiency which is due essentially to the realistic conditions that are not considered in the optical model such as: dirt effect, shading, changes in reflection and refraction selective coating incident angle effects.

## 5. Conclusions

A FVM for solving the RTE is coupled with an energy balance model to simulate the optical-thermal process of a PTC. The FVM is used to calculate the solar energy distribution on the absorber tube using a mesh that reduces the false scattering shortcoming. The simulation results are compared with numerical and experimental results from literature and it is shown that the predicted results follow the same trend. However, some differences in the solar distribution around the absorber tube are detected due to the false scattering and the modeling of the solar irradiation as a collimated beam. The optical model can be improved by taking into account the finite size of the sun which is important in such solar collectors and might require the use of the ray tracing method in the future investigations which avoid the false scattering problem. An additional factor, that considers realistic conditions such as dirt, shading and refraction, could be added to the optical model to give a more accurate solar distribution.

The numerical results have shown that of the solar flux distribution around the absorber can be divided in 4 general zones: the direct radiation zone, the heat flux increasing, the heat flux decreasing zone and the shadow effect zone. Furthermore, the model provides the temperature distribution on the absorber which is observed to follow the same distribution as the solar energy flux for the azimuthal direction. This distribution shows large difference of temperature of about 80ºC. This difference has an important effect on the thermal behaviour of the PTC which is not accounted for in simpler models, such as those where the solar energy flux is considered constant.

## 6. Acknowledgments

This work has been partially funded by the Spanish Agency of International Relations (AECI) and by the Ministerio de Educación y Ciencia, Spain (Project reference ENE2010-17801).

## 7. References


Chai, J.C., Lee, H.S., Patankar, S.V., 1994. "Finite volume method for radiation heat transfer". Journal of Thermophysics and Heat Transfer. 3,419-425.

Cheng, Z.D., He, Y,L., Xiao, J., Tao, Y.B., Xu, R.J., 2010. "Three-dimensional numerical studyof heat transfer characteristics in the receiver tube of parabolic trough solar collector". International communications in heat and mass transfer. 37, 782-787.

Colomer,G. and Borrell,R. and Lehmkuhl,O. and Oliva,A. 2010 "Parallelization of combined convection-radiation numerical" Proceedings of International Heat Transfer Conference14, IHTC14 ,Washington, DC, USA ,August, 8-13

Dudley, V. E., Kolb, G. J., Sloan, M., Kearney, D et al., 1994. "Test Results: SEGS LS 2 Solar Collector". SAND94-1884. Albuquerque, NM: SANDIA National Laboratories.

Duffie, J. A., Beckman, W. A., 1991. Solar Engineering of Thermal Processes, Second Edition, New York. Incropera, F., DeWitt, D.,1990. Fundamentals of Heat and Mass Transfer, Third Edition, New York, NY: John Wiley and Sons.

Forristall, R., 2003. "Heat Transfer Analysis and Modeling of a Parabolic Trough Solar Receiver Implemented in Engineering Equation Solver, Technical Report", NREL/TP-550-34169.

García-Valladares, O., Velázquez, N., 2009 "Numerical simulation of parabolic trough solar collector: Improvement using counter flow concentric circular heat exchangers". International Journal of Heat and Mass Transfer. 52, 597-609.

Guven, H.M., Bannerot, R.B., 1985. "Derivation of universal error parameters for comprehensive optical analysis of parabolic troughs". Proceedings of the ASME-ISES Solar Energy Conference, Knoxville, USA, 168–74.

He, Y-L; Xiao, J., Cheng Z-D., Tao, Y-B., 2011. "A MCRT and FVM coupled simulation method for energy conversion process in parabolic trough solar collector". Renewable Energy. 36, 976-985.

Odeh, S.D., Morrison, G.L., Behnia, M., 1998 "Modelling of parabolic trough direct steam generation solar collectors", Solar Energy. 62 (6), 395 406.

Jeter, M.S., 1987. "Analytical determination of the optical performance of practical parabolic trough collectors from design data". Solar Energy. 39 (1), 11–21.

Model 3001-03, 1981 Concentrating Solar Collector Commercial Brochure. Acurex Solar Corporation, Mountaain View, California .

Modest, M. F., 2003. Radiative Heat Transfer, McGraw-Hill, New York.

Price, H., Lüpfert, E., Kearney, D., Zarza, E., Cohen, G., Gee, R., 2002. "Advances in Parabolic Trough Solar Power Technology". Journal of Solar Energy Engineering. 124, 109-125.

Rabl, A., 1987. "Optical and thermal analysis of concentrators". In Proceedings of the solar thermal concentrating collector technology symposium. Report SERI/TP-34-048.

Raithby , G.D., Chui, E.H., 1990. "A finite-volume method for predicting a radiant heat transfer in enclosures with participating media". Journal of Heat Transfer. 112, 415-423.

Ratzel, A., Hickox, C., Gartling, D. 1979. "Techniques for Reducing Thermal Conduction and Natural Convection Heat Losses in Annular Receiver Geometries. " Journal of Heat Transfer. 101, 108–113.

Riveros, H.G., Oliva, A.I., 1986. "Graphical analysis of sun concentrating collectors", Solar Energy. 36 (4), 313–322